

Some SIF's evaluations by Dual BEM for 3D cracked plates

A. Apicella #, R. Citarella[^], R. Esposito*, A. Soprano*

Alenia un'Azienda Finmeccanica, Pomigliano d'Arco (NA), Italy

[^]Dept. of Ingegneria Meccanica, University of Salerno, via Ponte Don Melillo, 84084 Fisciano, Salerno, Italy

*Dept. of Progettazione e Gestione Industriale, University of Naples Federico II, P.le Tecchio 80, 80125 Napoli, Italy

Abstract

This work concerns a study on numerical evaluation of linear elastic crack 3D problems with linear and non-linear load conditions, using a Single-Domain Boundary Element Method and in particular the Dual Boundary Element Methodology (DBEM). The method, implemented in a commercial code (BEASY), uses both the conventional Displacement Integral Equation and the less commonly used Traction Integral Equation and relies on the use of discontinuous elements to model the cracks, whose Stress Intensity Factors (SIF's) are calculated by means of the Crack Opening Displacement method (COD). SIF's on a circular quadrant crack and a rectangular through crack have been evaluated with reference to single and two hole plates undergoing different linear and non-linear loading conditions.

Keywords: DBEM, contact analysis, crack.

1. Theoretical aspects of Dual Boundary Element method

There follows a summary of the Single-Domain Boundary Element Method [1,2] and in particular the Dual Boundary Element Methodology, detailed in references [3] for 2D and [4,5] for 3D applications, for the numerical evaluation of linear elastic crack problems using boundary integral equations with discontinuous elements. The method, very powerful in particular for crack propagation problems [6], uses both the conventional Displacement Integral Equation (the free term of which involves displacements at the source point) and the less commonly used Traction Integral Equation (the free term of which involves tractions at the source point). Actually, the displacement equation alone does not provide a viable method for single domain analysis of general crack problems, because of the stiffness matrix ill-conditioning (there is not a sufficient number of independent equations). This drawback can be circumvented adopting two independent equations on the two crack edges.

1.1 Boundary Integral Equations (BIE)

Define spatial coordinates x_i (subscript $i=1,2,3$), with source point x_i^* . Displacement $u_i(x)$ and traction $t_i(x)$ on the boundary S of a three-dimensional solid are related by the displacement BIE (1) and traction BIE (2) (three components $j=1,2,3$), for a source point on a smooth boundary S where the summation convention is assumed for repeated suffices:

$$\frac{1}{2} \delta_{ij} u_j(x^*) + \int_S \overline{T_{ij}(x^*, x)} u_j(x) dS(x) - \int_S \overline{U_{ij}(x^*, x)} t_j(x) dS(x) = 0 \quad (1)$$

$$\frac{1}{2} t_j(x^*) - n_i(x^*) \int_S \overline{D_{kij}(x^*, x)} t_k(x) dS(x) + n_i(x^*) \int_S \overline{S_{kij}(x^*, x)} u_k(x) dS(x) = 0 \quad (2)$$

This is a limiting form of the BIE characterised by a source point interior to the boundary S . The kernel functions $\overline{T_{ij}(x^*, x)}$ and $\overline{D_{kij}(x^*, x)}$ are $O(r^{-2})$ singular while $\overline{S_{kij}(x^*, x)}$ is

$O(r^{-3})$ singular. The two symbols \int_S^- , \int_S^+ stand respectively

for the Cauchy and Hadamard principal value integrals.

In the displacement and traction equation, there arise apparently singular terms due to the presence of the source point on the boundary. Provided that certain continuity conditions hold for the surface variables (displacement and traction) at the source point, no singularities actually exist and the integral equations are well defined.

2. Discontinuous elements

Application of conventional Boundary Element Method with continuous element to the hypersingular traction equation fails due to the unsuitable representation of the surface displacement and traction at the nodal source points. The numerical solutions will not converge unless the assumed form of displacement and traction on the boundary element adjoining the source point comply with the following conditions: displacement and traction assumed on the boundary elements must be respectively C^1 and C^0 -continuous at the boundary source point. The necessary conditions for the existence of the principal value integrals obtained in the derivation of the dual boundary integral equations impose restrictions on the discretization. Actually, in the traction equation the continuity requirements of the Hadamard principal value integral are satisfied (in a simple way) only by discontinuous elements, since all the nodes are internal points of the element where a continuous differential approximation is defined. Moreover, using the traction equation, the geometry smoothness requirement at a collocation point is implicitly satisfied by the discontinuous element.

3. Crack modelling

The general modelling strategy can be summarised as follows:

- the traction equation (2) is applied for collocation on one of the crack boundaries;
- the displacement equation (1) is applied for collocation on the opposite crack boundary and remaining boundaries;
- the crack boundaries are discretized with discontinuous boundary elements;

- continuous quadratic boundary element are used along the remaining boundaries of the problem domain, except at the intersection between a crack and an edge, where discontinuous or semi-discontinuous elements are required, in order to avoid nodes at the intersection.

4. Stress Intensity Factors (SIF's)

Discontinuous quadratic boundary elements are used along the crack front, and values of stress intensity factors (SIF's) are derived from the crack opening displacement method (COD) on such elements, by using the BEASY code [7] developed at the Wessex Institute of Technology (UK), well suited for 3D SIF's evaluation and automatic crack propagation [8].

5. Example solutions

A large square plate contains one or two cracked holes; its overall sizes are: $-B < x_1 < +B$, $-H < x_2 < +H$, $-h/2 < x_3 < h/2$, as shown in Figg. 1-2. Values of tensile modulus $E=72000 \text{ N/mm}^2$ and Poisson's ratio $\nu = .3$ are assumed. The hole radius is $R=2.0 \text{ mm}$ and, in the two hole case, the hole pitch is $P=20.0 \text{ mm}$. The plate dimensions $2B$ and $2H$ are chosen sufficiently large so as to simulate an infinite panel and the plate thickness is $h=1.6\text{mm}$.

Two structural configurations are considered:

1. A single hole plate, with a circular quadrant surface crack (Fig.1) of radius $a_1=1.2 \text{ mm}$ or $a_1=0.8 \text{ mm}$ and with a panel size of $2B=2H=80\text{mm}$ (adequate in order to approximate as infinite the plate with less than 1.5% SIF's variation);

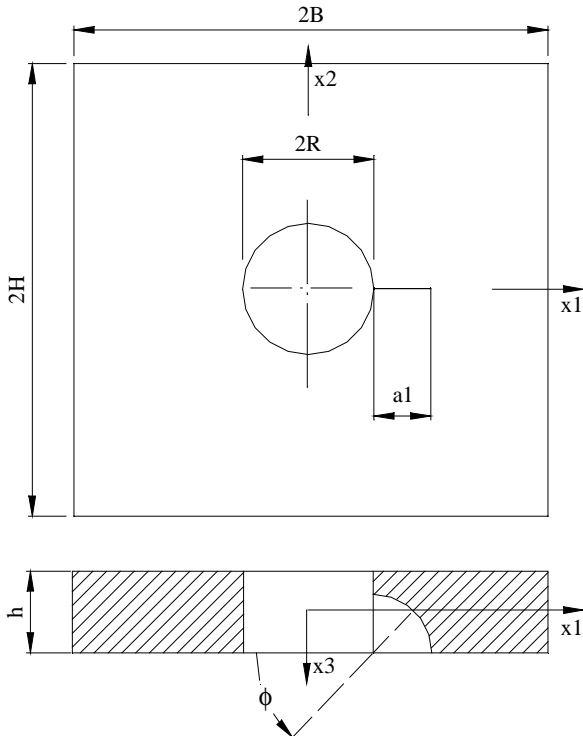


Fig.1: One hole plate with circular crack at a hole.

2. A two hole plate with a quadrant crack of radius $a_1=0.8 \text{ mm}$ and a nearby through-crack emanating from an adjacent hole (Fig.2) of length $a_2=8.0 \text{ mm}$, with a panel size

of $2B=2H=160\text{mm}$ (adequate in order to approximate as infinite the plate with less than 1.5% SIF's variation).

The loading cases considered for the one hole plate are (Fig.3):

- a) uniform remote tension $S=100 \text{ N/mm}^2$ applied as tractions on one end surface, whilst the other end surface is suitably constrained. SIF's values for the quadrant crack ($a_1=1.2 \text{ mm}$) are normalised by $K_0 = S\sqrt{\pi \cdot a_1 / Q}$, where $Q=2.464$ [9].
- b) uniform remote bending $\sigma_{22} = S (2 x_3 / h)$ each applied as tractions t_2 acting on the end surface $x_2=+H$ whilst the other end surface is suitably constrained. SIF's values for quadrant crack ($a_1=1.2 \text{ mm}$) are normalised as above;
- c) momentum of magnitude $M=F*3.2=5120 \text{ N*mm}$ ($F=1600 \text{ N}$), applied by means of a tilted pin, with the contact area modelled by gap elements. SIF's values for the quadrant crack ($a_1=0.8 \text{ mm}$) are normalised by $K_0 = S\sqrt{\pi \cdot a_1 / Q}$, where $Q=2.464$ [9]. In this load case the tension S is the hole bearing stress and is calculated as $S=F/(2*R*h)=250\text{N/mm}^2$.

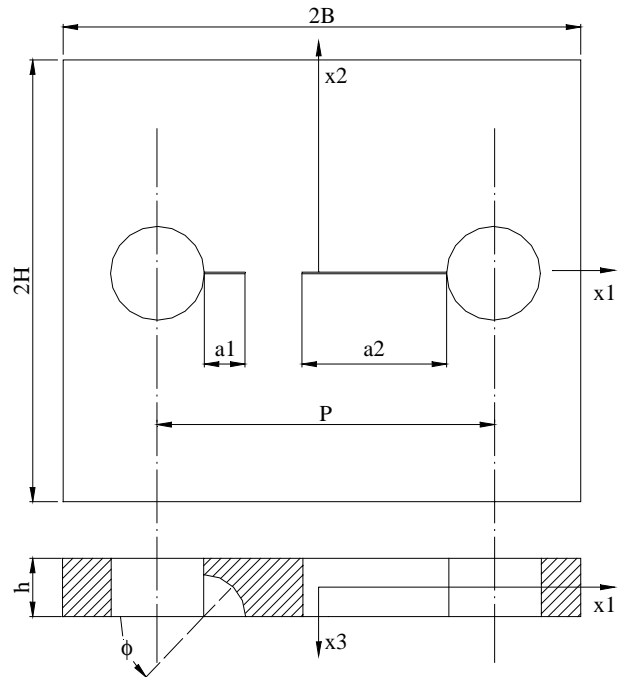


Fig. 2: Two hole plate with quadrant and through cracks.

The loading case considered for the two hole plate is (Fig.4):

- pin load of magnitude $F=1600 \text{ N}$, applied as body load in each pin (made of the same plate material) of the two-hole plate, with the contact area modelled by gap elements. SIF's values for the quadrant crack are normalised by $K_0 = S\sqrt{\pi \cdot a_1 / Q}$, where $Q=2.464$ [9]. SIF's values for the through crack are normalised by $K_0 = S\sqrt{\pi \cdot a_2}$. In this load case the tension S is the hole bearing stress and is calculated as $S = F / (2*R*h) = 250\text{N/mm}^2$ ($F=1600 \text{ N}$).

5.1 One hole plate results

For one-hole plate, in the case of uniform remote tension, tridimensional numerical solutions have been obtained using a total of about 990 linear elements, as in Fig.5, except on the cracks where “reduced” quadratic elements (8-noded elements) have been used in any case.

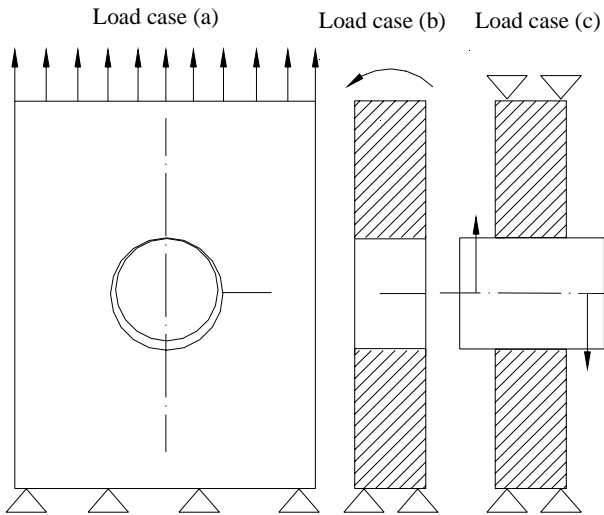


Fig.3: Loading conditions for the one hole plate.

This mesh corresponds to 6252 degrees of freedom (dof's) and run times were about 1 hour, on a PC Pentium 200 with 96 Mbyte of RAM. Increasing the order of the elements to “reduced” quadratics (7533 dof) around the crack, produced a slight SIF's variation (less than 2%) while run-times increased to 2 hours. Negligible changes (less than 1%) in the solution were produced by setting up the element subdivision option, applied to the most refined mesh adopted, capable to augment the number of Gauss quadrature points in quasi-singular integrations. Using an increased number of subdivisions in the angular and radial direction had a negligible effect on the results (moreover it would be possible to reduce the number of crack elements without affecting significantly the results). Normalised SIF's (K_I/K_0 , $K_0=124 \text{ Nmm}^{-3/2}$) for the quadrant crack, $a_1=1.2 \text{ mm}$, are given in Fig. 6. The mesh on the crack is based on 8 uniform divisions in the angular direction and 6 divisions in the radial direction as illustrated, together with Von Mises stresses for traction case, in Figg. 7a-b.

The same remarks hold for the bending case where the same mesh as above has been adopted but now it is necessary a p-convergence analysis up to quadratic elements (9-noded elements), in order to get good convergence results. Run times increased correspondingly to 4 hours for 8-noded elements (13623 dof) and 7 hours for 9-noded elements (16662 dof). Von Mises stress on the overall plate and in particular around the hole are illustrated in Figg. 8a-b. Normalized SIF's for the quadrant crack (K_I/K_0 , $K_0=124 \text{ Nmm}^{-3/2}$) are presented in Fig. 9. Von Mises stress and crack mesh are depicted in Fig. 10.

For tilted-pin case, the mesh adopted is based on 1190 elements varying from linear to quadratic in a p-convergence study. Such mesh is well evident from Figg. 11a-d, where deformed plots, representative of the stress state, are magnified by a factor of 15. The analysis is non linear and an iterative-incremental procedure is adopted. Run times were

varying between 30 hours with 9840 dof (2778 contact dof) and 57 hours with 15363 dof (2778 contact dof). In Figg. 12-14 SIF's (K_I/K_0 , K_{II}/K_0 , K_{III}/K_0) are depicted. In this case there is a mixed load condition even if the mode I of load is prevailing.

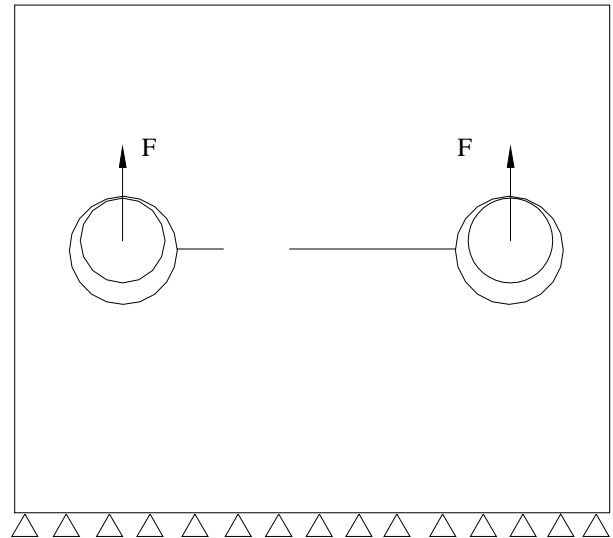


Fig. 4: Loading condition for the two hole plate.

5.2 Two hole plate results

For two hole plate, the boundary element mesh used for the quadrant crack corresponds to 6 uniform divisions in the angular direction and 4 divisions in the radial direction, whilst for the through crack it corresponds to 6 uniform divisions in x_3 direction and 5 divisions in x_1 direction. The plate boundary mesh is easily obtained.

For pin-loading case, linear elements have been used throughout the plate surface, except in the zone surrounding the two holes, including the two loaded pins, modelled with “reduced” quadratic elements. In this contact problem, modelled with gap elements on the interface area, the analysis is non-linear because of a changeable contact area with a gradually increasing load and it is worked out by an iterative-incremental procedure. Run time were varying between 10 hours, with 2149 elements (13629 dof and 1416 contact dof), to 40 hours, with 2200 elements (18525 dof and 1944 contact dof). In Figg. 15a-c are illustrated normal tractions on pin-hole contact area (it is evident they are zero in the disconnected part). Normalized SIF's for the quadrant cracks are depicted in Fig. 16a, and those for the through cracks in Fig. 16b. In Fig. 17 Von Mises stress are well evident around the cracks whose opening in the deformed plate is showed too.

The plate boundary mesh is illustrated in Fig. 18.



Fig. 5. Overall boundary mesh for the one hole plate.

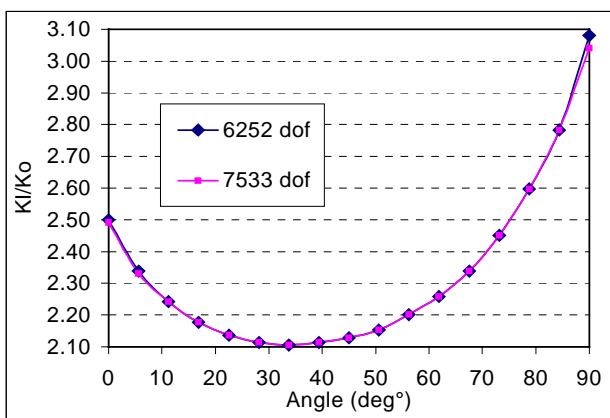


Fig. 6. Normalized SIF's for the one hole plate in traction case.

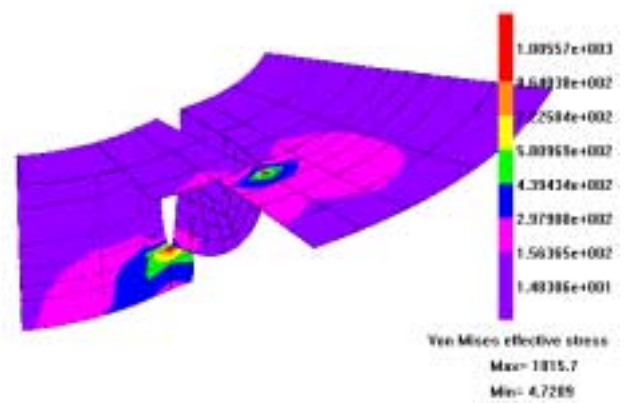


Fig. 7a. Close-up of the crack element mesh and stress state.

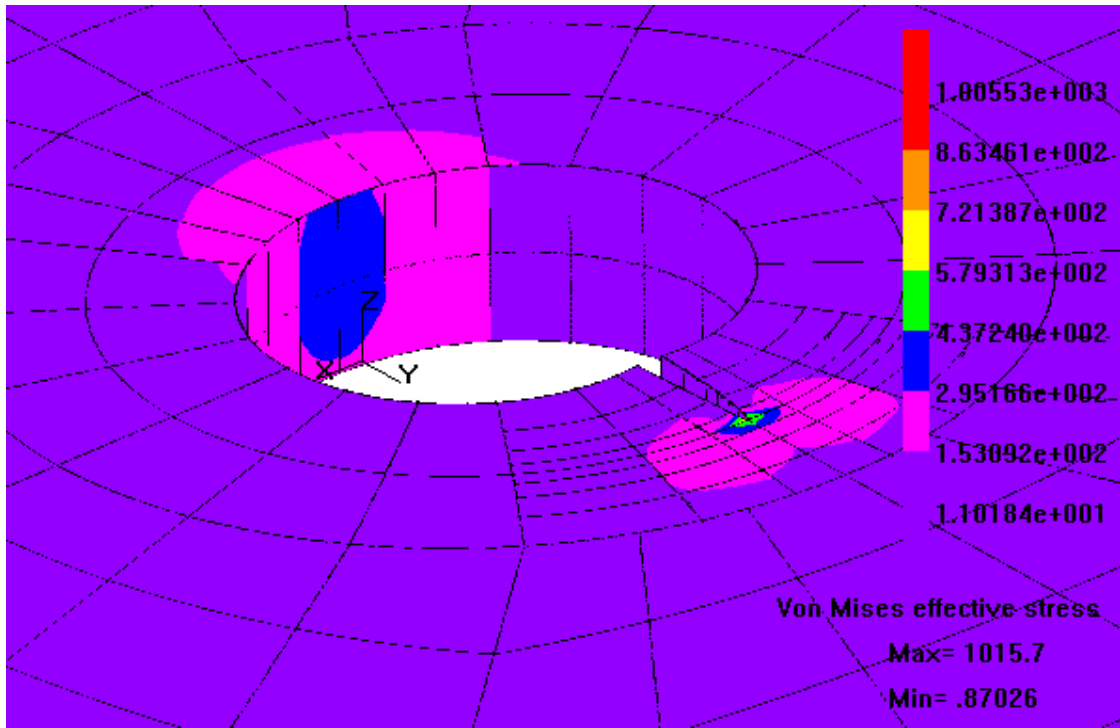


Fig. 7b. Close-up of the hole mesh and Von Mises stress state.

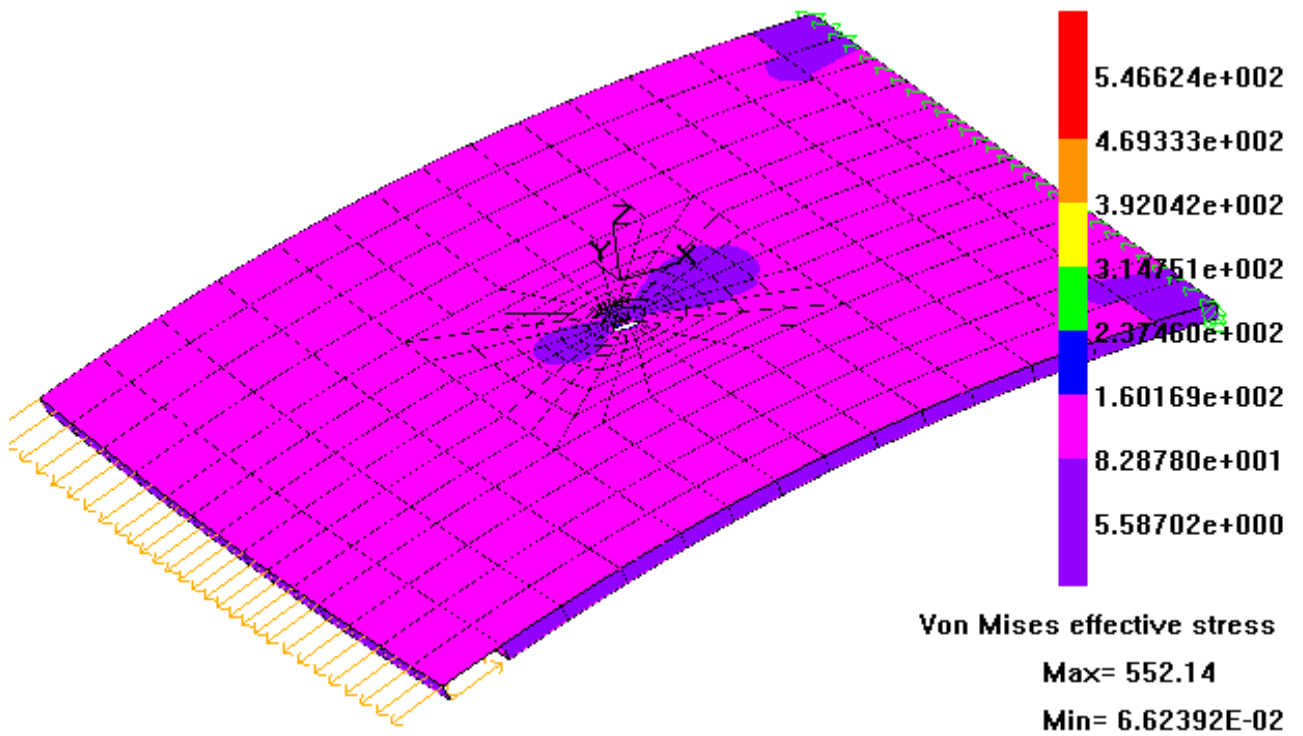


Fig.8a. Overall stress state on the one hole plate deformed plot, in bending case.

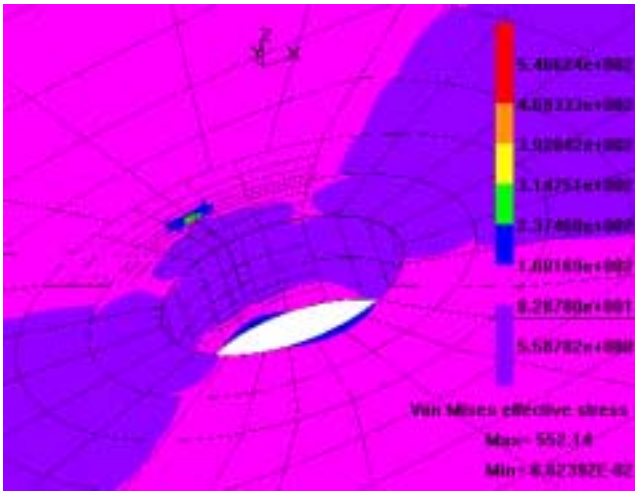


Fig. 8b. Close-up of the stress state around the hole (R=2mm).

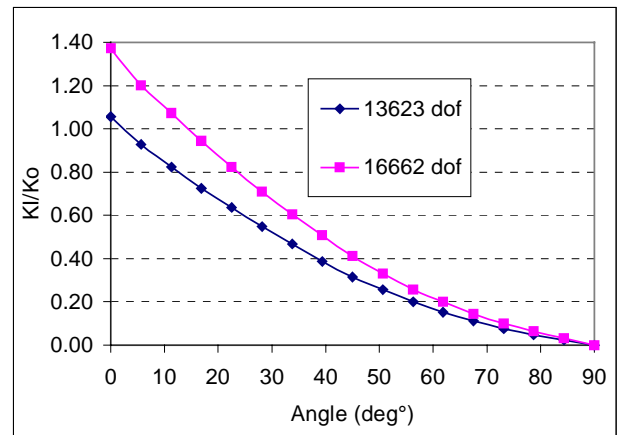


Fig.9. Normalized SIF's (K_I / K_0 , $K_0=124 \text{ Nmm}^{-3/2}$) for the one hole plate in bending case.

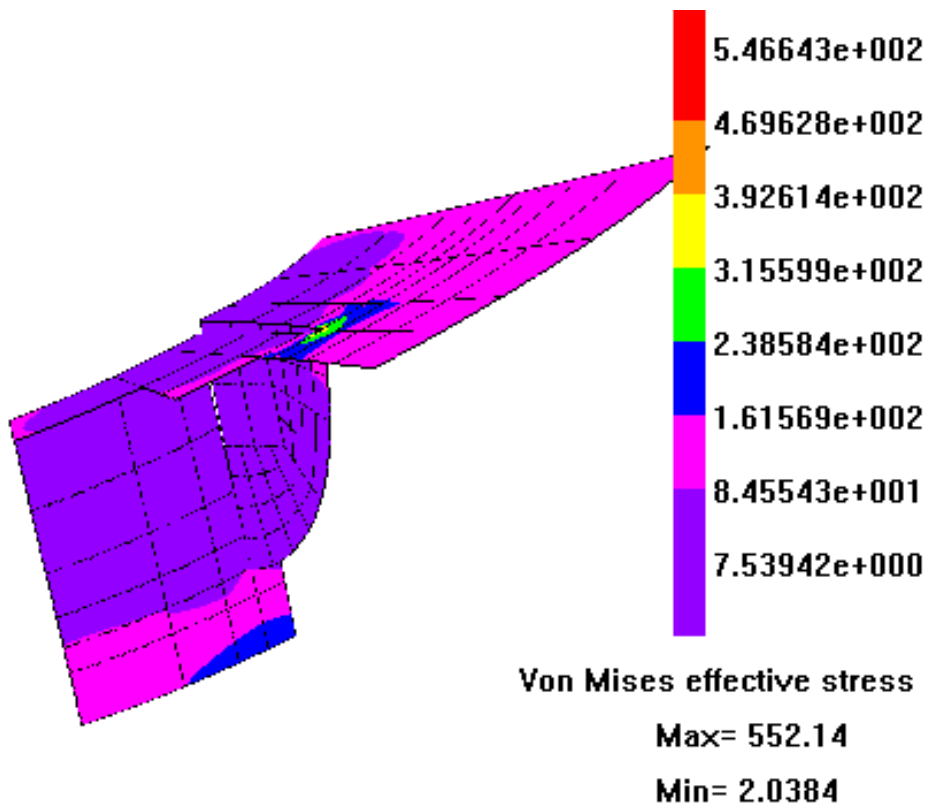


Fig. 10. Stress state around the crack ($a=1.2$), in bending case.

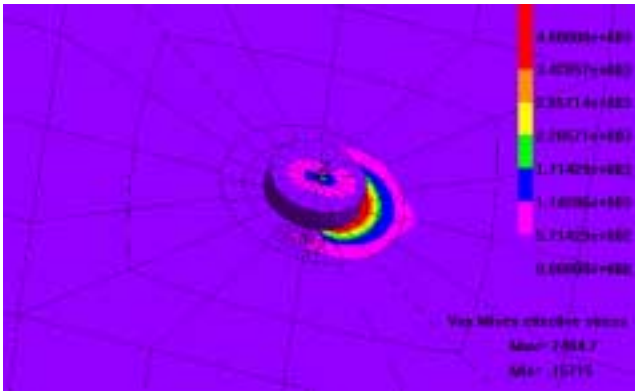


Fig. 11a. Close up of the stress state for a tilted pin ($M=5120$ Nmm, $a_1=0.8$ mm) in the one hole plate.

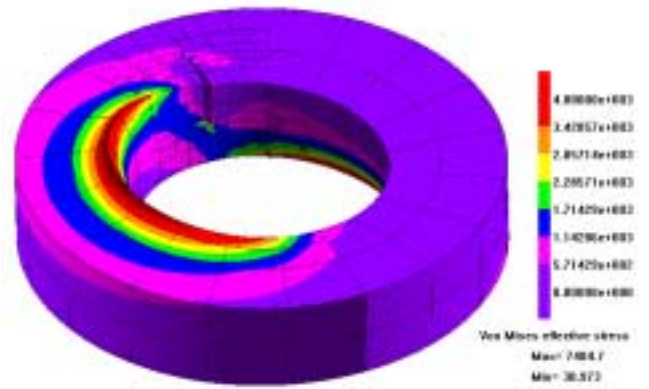


Fig. 11d. Close-up of the hole surface contact stress on one hole plate deformed plot.

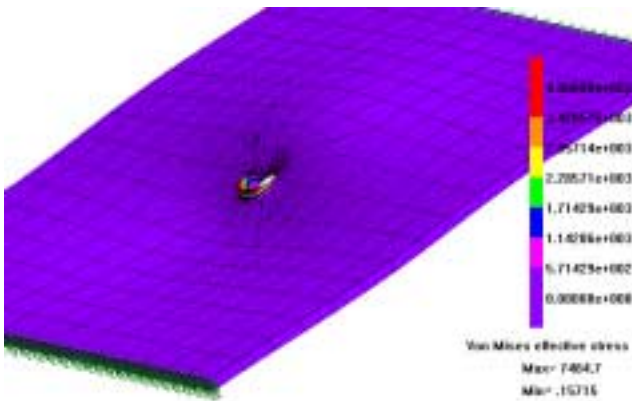


Fig. 11b. Stress state on a deformed plot, for a clamped plate undergoing momentum.

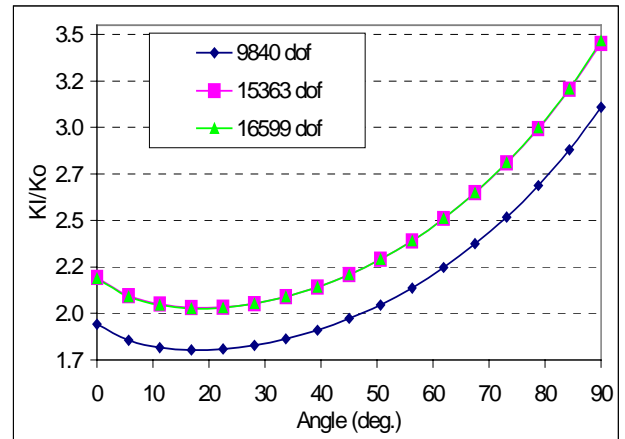


Fig. 12. Normalized SIF's (KI/Ko , $Ko=252$ Nmm^{-3/2}, $a_1=0.8$ mm) in tilted pin case.

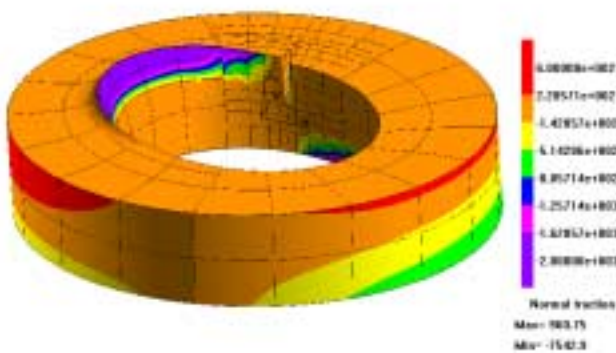


Fig. 11c. Close-up of the hole contact pressure on one hole plate deformed plot.

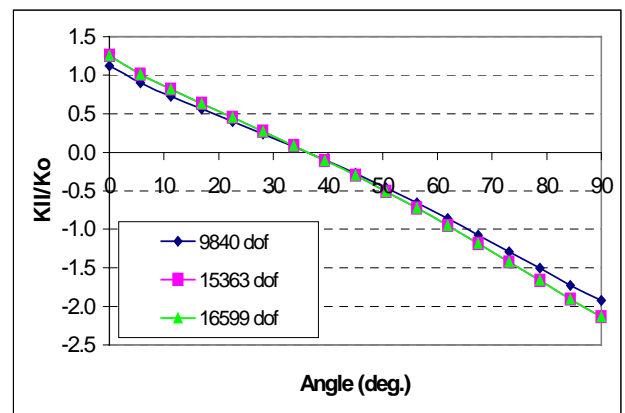


Fig. 13. Normalized SIF's (KII/Ko , $Ko=252$ Nmm^{-3/2}, $a_1=0.8$ mm) in tilted pin case.

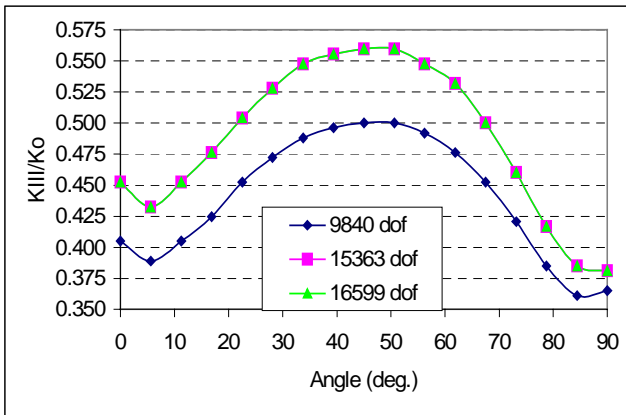


Fig. 14. Normalized SIF's (K_I/K_0 , $K_0=252 \text{ Nmm}^{-3/2}$, $a_1=0.8\text{mm}$) in tilted pin case.

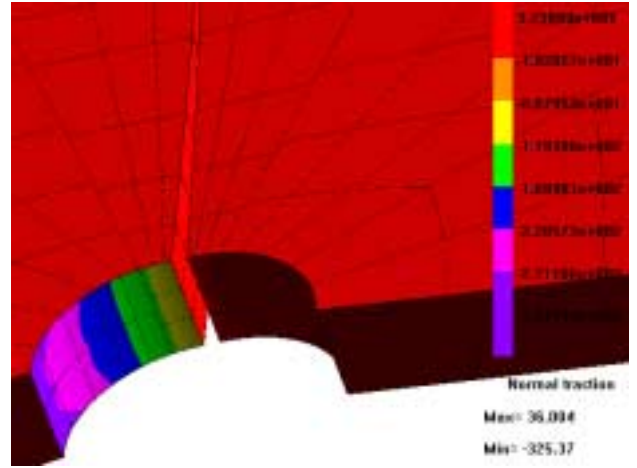


Fig. 15c. Pin bearing traction on the deformed contact area for the pin-loaded two hole plate.

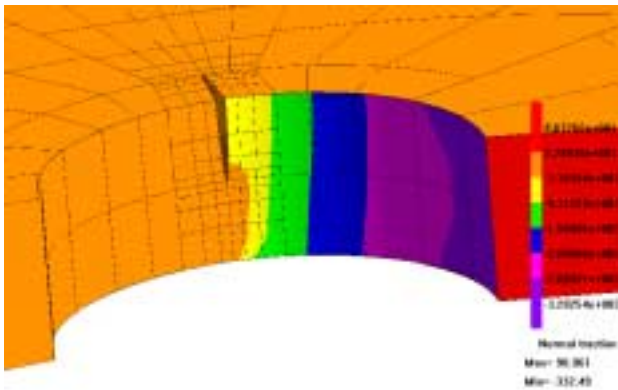


Fig. 15a. Hole bearing traction on the deformed contact area for the pin-loaded two hole plate.

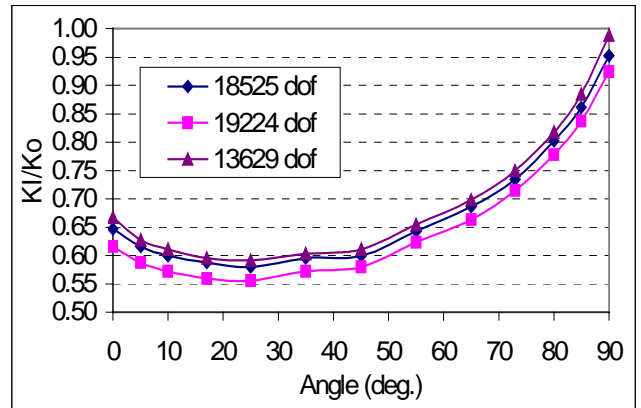


Fig. 16a. Normalized SIF's ($K_0=252 \text{ Nmm}^{-3/2}$) for quadrant crack of the pin-loaded plate.

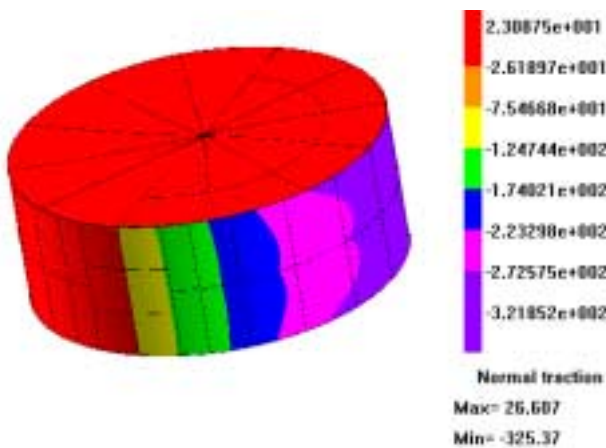


Fig. 15b. Pin bearing traction on the deformed contact area for the pin-loaded two hole plate.

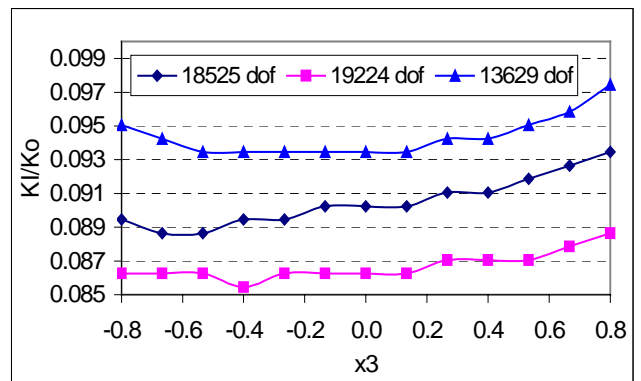


Fig. 16b. Normalized SIF's ($K_0=1252 \text{ Nmm}^{-3/2}$) for through crack of the pin-loaded plate.

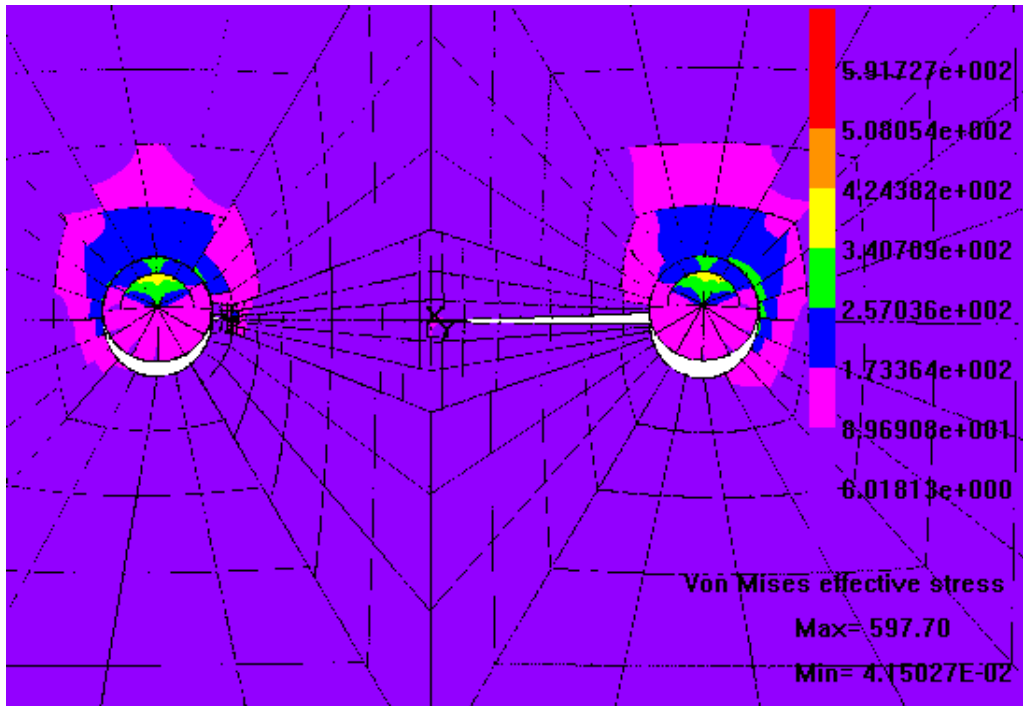


Fig. 17. Stress state around the deformed holes of the pin-loaded plate ($F=1600$ N on each pin).

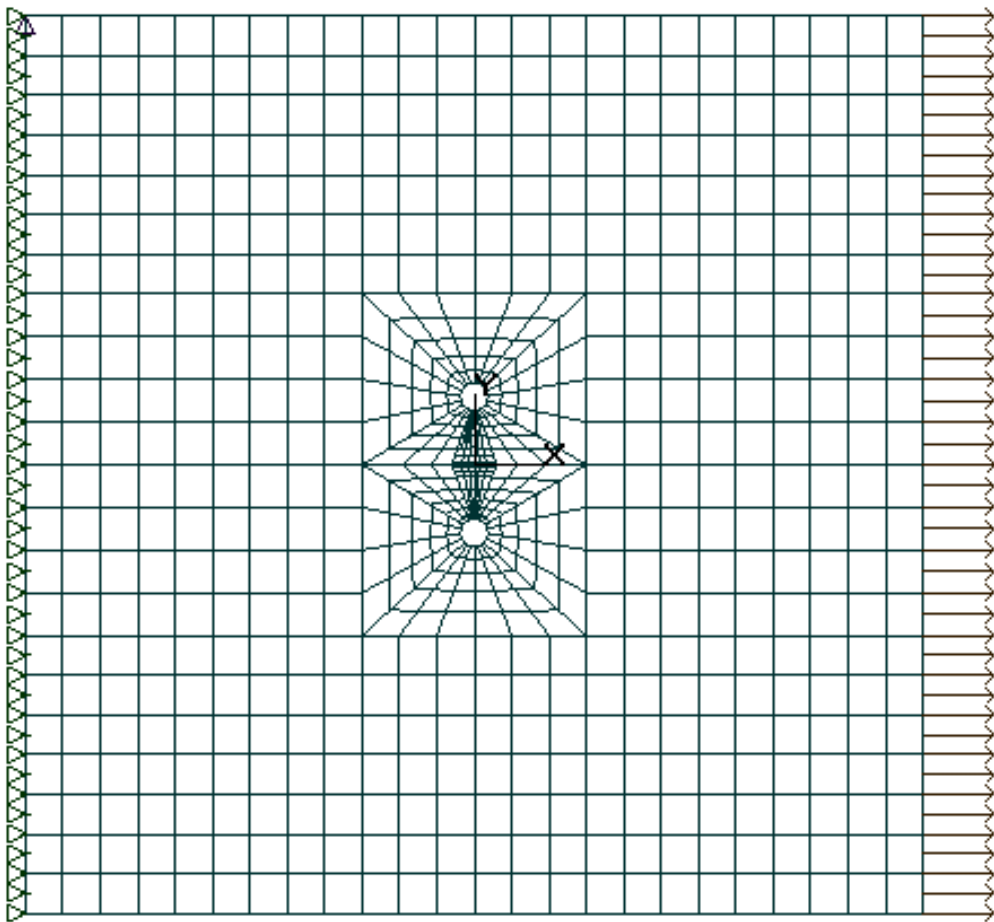


Fig. 18. Overall boundary element mesh used for the two hole plate, in bending case.

5.3 Multi region formulation

Since the procedures developed for FEM generally assume a particular type of matrix, i.e. symmetric, positive definite (SPD), sparse with small bandwidth, new solution strategies are required to solve the different types of matrix produced by BEM.

In the construction of large, complex models it is often more economical to split the model into smaller simpler sub-models. These sub-models or regions, which may also have different material properties, are modelled independently and then joined together along an interface. This strategy leads to an overall system matrix which has a blocked, sparse and unsymmetric character. This characteristic of multi-region formulation significantly extends the range of problems that can be solved, due to the large savings in storage and CPU calculations, required to solve the matrix, compared with the case of a fully populated matrix. However, the sparsity of such matrices is of a different type than that of FEM matrices. This has led to research being concentrated on the direct method for solving matrices, characterised by the factorisation of the system matrix by Gauss elimination or by Choleski's method. As a matter of fact a direct method is implemented in BEASY code for system matrices resolution.

6. Conclusions

In conclusion some further remarks are due with regard to the opportunity, with a DBEM procedure, to model the zone surrounding the cracks with discontinuous elements, in such a way to simplify the meshing process and without loss of accuracy. Moreover it has been possible to reduce run times and storage required, by zoning the whole plate in an adequate number of parts (paying attention to number consecutively the adjacent zones, in order to maximize benefits). Cubic elements have also been tried in the zone surrounding the cracks but without any improvement in accuracy. A satisfactory agreement of the results has been obtained compared with SMAAC partner [10,11] with a relatively small modelling effort. Further improvement in the BEASY code will be necessary in order to lighten computational times, even if we have to point out that the reported run-times are pessimistic because obtained with a compressed and highly fragmented disk.

References

- [1] M.H. Aliabadi and D.P. Rooke, "Numerical Fracture Mechanics", Computational Mechanics Publications, Southampton (UK), 1992.
- [2] M.H. Aliabadi, C.A. Brebbia, "Advances in Boundary Element Methods for Fracture Mechanics", Computational Mechanics Publications, Southampton (UK), 1992.
- [3] Portela A., Aliabadi M.H. & Rooke D.P. "Dual Boundary Incremental Analysis of Crack Propagation", Int Journal Computers and Structures, Vol.46, pp 237-247, 1993.
- [4] Mi, Y., Aliabadi, M.H., "Dual Boundary Element Method for Three Dimensional Fracture Mechanics Analysis", *Eng. Analysis with Boundary Elements*, Vol 10, 1992.
- [5] Mi Y., Aliabadi M.H., "Three-dimensional crack growth simulation using BEM", *Computers & Structures*, Vol 52, No 5, pp 871-878, (1994).
- [6] A. Apicella, R. Citarella, R. Esposito, "Sulla previsione della propagazione per fatica di cricche multiple tramite elementi di contorno discontinui", Proceedings of XXIII Convegno Nazionale AIAS, Rende, 1994.
- [7] Beasy Crack Growth Guide Book, Computational Mechanics BEASY, Ashurst, Southampton, 1994.
- [8] A.C. Neves, R.A. Adey, J. M. W. Baynham and S. M. Niku, "Automatic 3D crack growth using BEASY", Proceedings of BEM 19 Conference, pp 819-827, Computational Mechanics Publications, Southampton, U.K. (1997).
- [9] P.W. Tan, J.C. Newman Jr and C.A. Bigelow "Three-dimensional finite element analysis of corner cracks at stress concentration", *Engineering Fracture Mechanics* 55, 502-505 (1996).
- [10] J.P.M. Goncalves, P.T. de Castro, "Contribution to the Numerical Modeling of a Corner Crack at a Fastener Hole", Document No. SMAAC-WP-2.0-09-1.1/IDMEC.
- [11] A. Young, "Single-Domain Boundary Element Method for 3-D Elastostatic Crack Analysis", Document No. SMAAC-WP-2.0-07-1.0/DRA.